

## Supplementary Information for

# “Interactions between C and Cu atoms in single-layer graphene: direct observation and modelling”

Emi Kano,<sup>\*ab</sup> Ayako Hashimoto,<sup>abcd</sup> Tomoaki Kaneko,<sup>e</sup> Nobuo Tajima,<sup>e</sup> Takahisa Ohno,<sup>e</sup> and Masaki

Takeguchi<sup>abc</sup>

- a. Graduate School of Pure and Applied Sciences, University of Tsukuba, 1-1-1 Tennodai, Tsukuba, Ibaraki 305-8573, Japan.
- b. Surface Physics and Structure Unit, National Institute for Materials Science, 1-2-1 Sengen, Tsukuba, Ibaraki 305-0047, Japan.
- c. Transmission Electron Microscopy Station, National Institute for Materials Science, 1-2-1 Sengen, Tsukuba, Ibaraki 305-0047, Japan.
- d. Global Research Center for Environment and Energy based on Nanomaterials Science, National Institute for Materials Science, 1-2-1 Sengen, Tsukuba, Ibaraki 305-0047, Japan.
- e. Computational Materials Science Unit, National Institute for Materials Science, 1-1 Namiki, Tsukuba, Ibaraki 305-0044, Japan.

\* Address correspondence to [KANOU.Emi@nims.go.jp](mailto:KANOU.Emi@nims.go.jp)

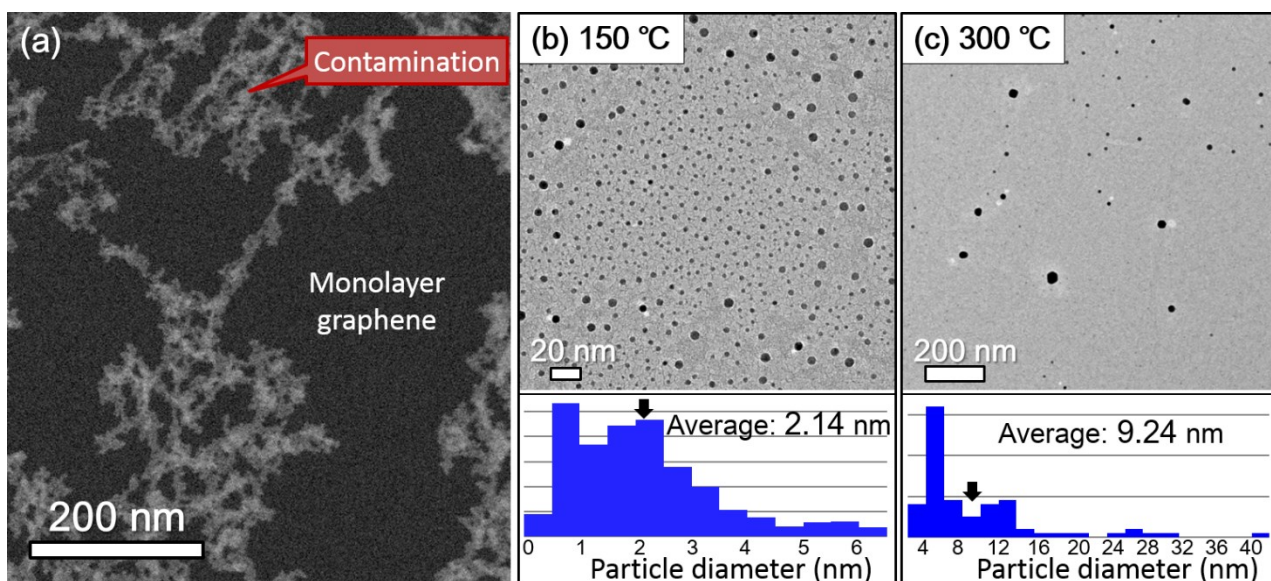


**Figure S1 Selecting observation areas.** (a) Low-magnification STEM image taken before the Cu deposition. The sample was heated in a vacuum at above 400 °C to create clean graphene patches  $\sim 200 \times 200$  nm<sup>2</sup> in size. After the Cu deposition, the sample was further heated at (b) 150 °C and (c) 300 °C. Corresponding particle size distributions are shown below the images. Cu atoms formed larger nanoparticles on contamination, as seen in the peripheral image areas in (b); therefore, further observations were carried out near the centres of the clean patches.

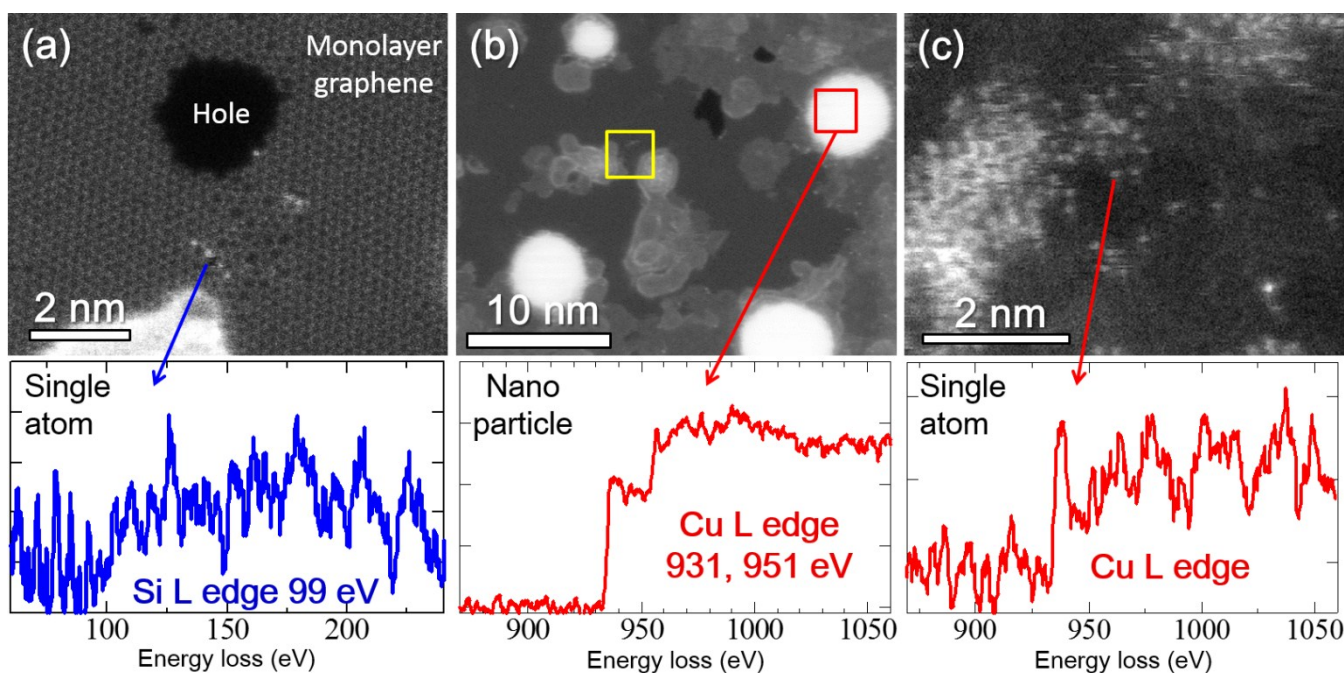


**Figure S2 STEM-EELS data for Si and Cu.** (a) Single Si atom detected before the Cu deposition. Si-contaminating areas were excluded from further examination. After the Cu deposition, Cu was detected at (b) all the nanoparticles around the observed area (yellow frame marks the area shown in Figs. 1a and 2a) and (c) single atoms dispersed in/on the graphene.

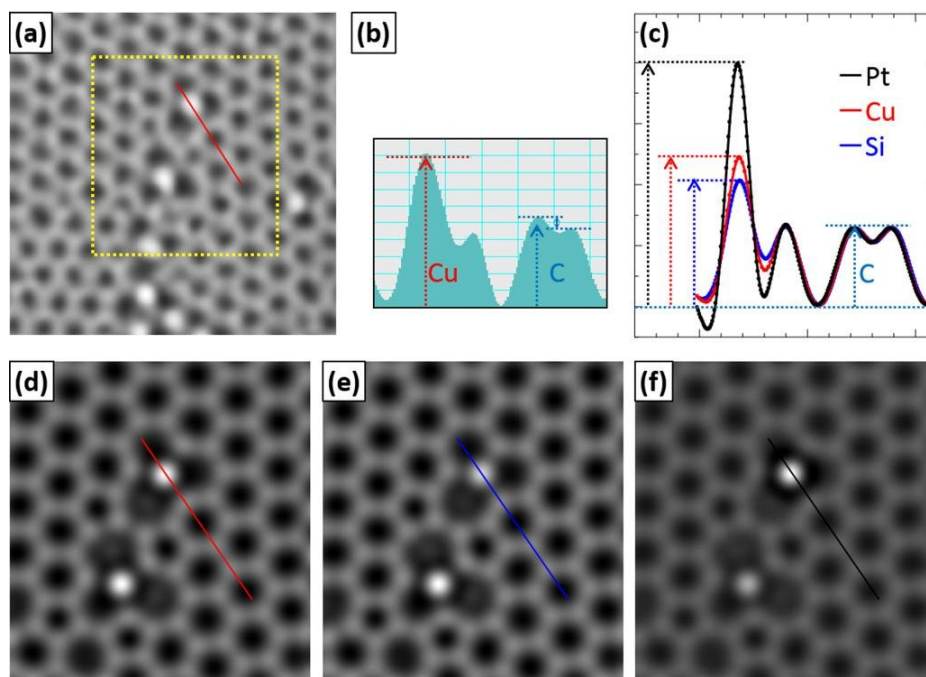


**Figure S3 TEM contrast.** (a) Experimental TEM image. (b) Signal intensity along the red line in (a). Cu/C ratio ranges from 1.73 to 2.00, due to the variation of C signal intensity. (c) Signal intensities along lines in panels (d–f), which show simulated TEM images of Cu, Si, and Pt, respectively. These models are similar to the structure marked by the yellow rectangle in (a). The lower-left bright atoms are Cu in all three cases, and only the upper-right bright atoms are changed. We used the multislice software xHREM<sup>TM</sup> from HREM Research Inc. under the following conditions: defocus spread 4 nm, beam convergence 0.3 mrad, third-order spherical aberration coefficient  $-0.001$  mm, fifth-order spherical aberration coefficient  $0.001$  mm, and defocus value 3 nm. The line profiles are normalized by C signals. The Cu/C, Si/C, and Pt/C signal ratios are 1.92, 1.62, and 3.15, respectively. Si should be a little darker than Cu, but the difference is hard to detect. Si was excluded using more sensitive EELS measurements (Figure S2).

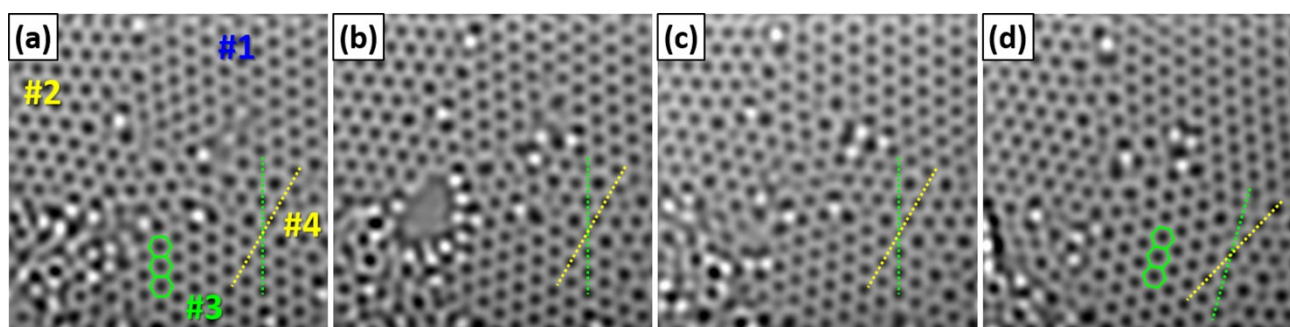


**Figure S4 Selected snapshots related to Figs. 2c–d and Movie S1.** Low-pass filtered TEM images indicate the rotation of grain #3. Panels (a–c) show the formation and mending of a nanopore in graphene. Movie S1 started just before the mending shown in (c). Green and yellow dotted lines indicate the orientations of grains #3 and #4, respectively. A part of grain #4 had an orientation differing by  $30^\circ$  from that of grain #3; grain #3 gradually rotated with that part of grain #4.

					Lifetime (s)	Structure	Transformation type
<b>(a)</b>	<b>(b)</b>	<b>(c)</b>	<b>(d)</b>	a	5	5566	<b>C -1</b>
				b	9	667	<b>C-C #1</b>
				c	6	667	<b>C-C #1</b>
				d	6	667	<b>C -1</b>
<b>(e)</b>	<b>(f)</b>	<b>(g)</b>	<b>(h)</b>	e	8	5657	<b>C-C #1</b>
				f	2	5666	<b>C-C #1</b>
				g	1	5567	<b>C -1</b>
				h	6	6-10	Mix
<b>(i)</b>	<b>(j)</b>	<b>(k)</b>	<b>(l)</b>	i	15	667	<b>C-C #1</b>
				j	1	666	Mix
				k	1	567	Mix
				l	1	668	Mix
<b>(m)</b>	<b>(n)</b>	<b>(o)</b>	<b>(p)</b>	m	1	668	Mix
				n	1	667	<b>C-Cu</b>
				o	2	677	<b>C-Cu</b>
				p	1	667	<b>C-C #2</b>
				q	2	668	Mix
<b>(q)</b>	<b>(r)</b>	<b>(s)</b>	<b>(t)</b>	r	1	678	<b>C-C #1</b>
				s	1	777	<b>C-C #1</b>
				t	5	678	<b>C-C #1</b>
				s	3	777	<b>C-C #1</b>
				t	1	678	<b>C-C #1</b>

**Figure S5 Snapshots and details of Movie S2.** Low-pass filtered TEM images at electron beam current density of 900 A/cm<sup>2</sup>. They were converted into Movie S2 with an arbitrary speed of 1 frame/s. Actual lifetimes of the imaged structures are listed in the table. “Mix” in the right column means that several transformations occurred in parallel (transformation types are shown in Fig. 3). C ejection changed the local coordination from three to four. As shown in panels (r–t), structures 678 and 777 appeared repeatedly with C-C rotation #1.

**(i) Metal atom @ Single vacancy (SV)**



**(ii) Cu atom @ Double vacancy (DV)**

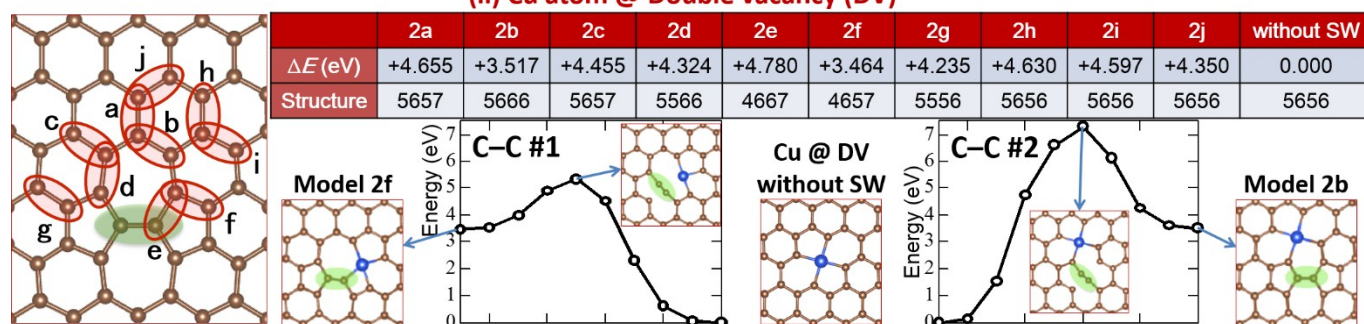


**Figure S6 DFT calculations.** When a metal atom substitute one (two) C atom at the positions indicated by the blue (red) rings, it forms three (four) coordinated structures with the neighbouring C atoms. We compared the energy difference  $\Delta E$  between the structures with and without Stone-Wales (SW) defects. (i)  $\Delta E$  data for single vacancy (SV) with a nearby metal atom, revealing larger values for Fe, Cr, Ni and Co (green table) than for Cu (blue table). Activation energy barriers of the models 1b, c, and d are shown in Fig. 4 of the main article. (ii)  $\Delta E$  data for Cu at double vacancy (DV), and energy diagrams of C–C rotations #1 and #2. As described in the main article, the energy barrier was smaller for C–C rotation #1 than #2; however, both rotations required higher energy at DV than at SV because of the larger distance between the rotating C atoms and Cu atom.

Structure	125 A/cm <sup>2</sup>	250 A/cm <sup>2</sup>	900 A/cm <sup>2</sup>	1500 A/cm <sup>2</sup>
667	56	22	7	4
677	59	21	5	4
668	37	13	5	8
577	19	8	3	7
568	-	4	9	6
666	60	20	6	3
5656	58	14	78	6

More than 30 s ← → Less than 10 s

**Table S1 Averaged lifetimes of typical structures at 150 °C.** Focusing the electron beam reduced the lifetime. At low beam currents, 577 and 568 disappeared twice faster than other structures due to the large stress from the pentagon they contained. Red numbers correspond to single, irreproducible measurements.

(a)	(b)	(c)		Lifetime (s)	Structure
			a	6	5555-6-7777
			b	3	555-777
(d)	(e)	(f)	a	5	5555-6-7777
			c	2	555-777
			d	72	5555-6-7777
			e	3	555-777
			f	5	555-777
(g)	(h)	(i)	g	5	585
			f	11	555-777
			h	2	555-777
			f	1	555-777
			i	1	585

**Figure S7 Snapshots and details of Movie S3.** Low-pass filtered TEM images taken from the first half of Movie S3. Bond rotations were often observed at the double vacancy or larger vacancies without Cu atoms. The reconstructed double vacancy of 5555-6-7777 was the most stable structure<sup>1</sup>. The structures 555-777 easily rotated as shown in panels (e,f). Eight- or nine-membered rings were created by the ejection of carbon atoms, followed by distortion or rotation of bonds. The latter half of Movie S3 shows the formation and reconstruction of another defect structure near the first defect (a–i).

## Supplementary references

- 1 A. W. Robertson and J. H. Warner, *Nanoscale*, 2013, **5**, 4079–4093.